PAPER

Assessment of equilibrium field coil misalignments on the divertor footprints in NSTX-U

IOP Publishing | International Atomic Energy Agency Nuclear Fusion

Nucl. Fusion **59** (2019) 076039 (16pp) https://doi.org/10.1088/1741-4326/ab1ee0

Assessment of equilibrium field coil misalignments on the divertor footprints in NSTX-U

S. Munaretto[1], T.E. Evans[1], N.M. Ferraro[2], D.M. Orlov[3], G.L. Trevisan[1,4] and W. Wu[1]

[1] General Atomics, PO Box 85608, San Diego, CA 92186-5608, United States of America
[2] Princeton Plasma Physics Laboratory, 100 Stellarator Rd, Princeton, NJ 08540, United States of America
[3] University of California—San Diego, 9500 Gilman Dr, La Jolla, CA 92093, United States of America
[4] Oak Ridge Associated Universities, 100 ORAU Way, Oak Ridge, TN 37830, United States of America

E-mail: munarettos@fusion.gat.com

Received 24 January 2019, revised 8 April 2019
Accepted for publication 2 May 2019
Published 12 June 2019

Abstract

The presence of error fields in a tokamak device is inevitable, so it is of fundamental importance to understand their impact on the operation of the device and up to what level they can be tolerated. In this paper a prediction of the impact on the magnetic footprints on the divertor plates due to the misalignment of NSTX-U equilibrium coils is presented. Resistive MHD simulations are used to predict the magnetic field perturbations experienced by the field lines due to the presence of error fields. A linear relation between the magnitude of the misalignment and the area of the magnetic footprints is found, as well as an inverse proportionality between the size of a magnetic footprint and the plasma penetration of the field lines composing the footprint. This study is intended as a starting point in the process of investigating divertor footprints associated with the plasma response to intrinsic error fields with resistive MHD codes. A basic interpretation of the results suggests that large footprints resulting from equilibrium coils misalignment may be desirable, to some extent, to decrease the peak heat load on the divertor components. A more complete interpretation of the results presented here will involve a number of complex physics issues, for example pedestal transport and stability, along with the role of various scrape-off layer and divertor processes, as well as experimental data to confirm the predictions.

Keywords: MHD, magnetic footprints, error fields

(Some figures may appear in colour only in the online journal)

1. Introduction

Although much work has been done to quantify and to minimize the perturbations due to non-axisymmetric magnetic field caused by intrinsic field-errors [1–5], they are intrinsically unavoidable in practical tokamak construction due to engineering tolerances, thermal stresses, coil feeds and small mechanical vibrations. It is therefore important to determine limitations in size and type of error fields allowable in the construction phase of a tokamak device, that is also a primary constraint in the cost of a machine. Included among the detrimental effects that error fields have on the plasma are: the loss of confinement due to mode locking [6, 7], and non-axisymmetric magnetic field perturbations that cause complex 3D edge magnetic topologies, significantly altering the properties of the heat and particle flux distributions on the divertor target plates [8–11]. Although, to a first approximation, spreading the heat and particle flux over a larger area seems desirable, it can be problematic if it spreads out of the designated areas (an example could be the presence of heat fluxes that exit the

Tungsten region and strike the Beryllium tiles in ITER), or if it leads to clustering of field lines and thus local peaks in heat deposition [12]. Understanding the physics mechanism that controls the heat and particle fluxes on the wall of a tokamak device is therefore of fundamental importance to ensure its operability and desired lifetime.

Due to several technical issues, the NSTX-U device [13] is going through a recovery phase [14]. These activities are expected to enable the 2 MA, 1 T, 5 s flat-top operation with neutral beam heating up to 10 MW to support the full range of physics research envisioned for the upgraded NSTX facility. The replacement of the 6 inner poloidal field coils and the upgrade of some of the plasma facing components are among the recovery activities. In particular new graphite plasma facing components are being implemented, to meet stringent heat flux and disruption requirements. This consists of a series of tiles designed to handle high heat fluxes (inboard divertor regions and part of the outer divertor region) and other designed to whithstand large disruption loads, but reduced thermal demands.

The main driver for the study presented here is the need to understand the impact that errors in the installation of the equilibrium coils have on the operation of the device. Since the interpretation of the results presented here involves a number of complex physics issues, this study is intended as a starting point in the process of investigating physics effects associated with pedestal transport and stability along with the role of various scrape-off layer and divertor processes for controlling heat and particle flux distribution associated with detached and radiating divertor and pedestal plasmas. In an ideal poloidal diverted plasma, the magnetic separatrix divides the magnetic field lines that are confined in the plasma from the open field lines that intersect the divertor target plates within relatively short distances. The presence of small non-axisymmetric perturbations generates a splitting of the separatrix into a pair of intersecting invariant manifolds known as homoclinic tangles [15–17] that allow magnetic field lines from within the plasma to reach the divertor target plates. The distribution of the magnetic field lines from within the plasma on the divertor plates has a well-defined toroidal structure, and it is dubbed magnetic footprint.

The work presented in this paper is focused on the area of the magnetic footprints due to the presence of error fields caused by the misalignment of equilibrium coils on NSTX-U, to determine the precision required to install them in order to contain the heat flux on the designated tiles. Of all the possible misalignments (shifts, tilts, out-of-plane deformations, non-circular effects, etc) associated with the equilibrium coils that may have a significant effect on the footprints, the focus of this work is on shifts and tilts. This study represents the first detailed investigation of these effects based on the linear resistive MHD plasma response to intrinsic error field. Experimental validation studies and non-linear MHD modeling, in order to assess the physics in the MHD model and to provide insight into the importance of other physics effects not included in the results discussed here, will be needed in future studies.

The 3D effect of the intrinsic error fields due to tilts and shifts of the poloidal and toroidal field coils on the axisymmetric equilibrium and on the plasma response is simulated using the linear, single fluid version of the resistive MHD code M3D-C1 [18–20]. The resulting perturbed equilibrium is then used by the GPU accelerated version of the field line integration code TRIP3D [21, 22] to estimate its impact on the edge topology of the plasma and the magnetic footprints. To perform the study, a model unperturbed NSTX-U equilibrium representing a high-performance and a high heat flux to the divertor discharge was chosen. The equilibrium is characterized by a plasma current of 2 MA, a toroidal magnetic field on axis of 1 T, a β_N of 4.2 and a q profile ranging from $q_0 = 3.1$ to $q_{95} = 6.68$ with a minimum of $q_{\min} = 2.2$ at the normalized flux coordinate $\psi_N = 0.18$. These calculations show that in a double null NSTX-U plasma a 5 mrad tilt of one of the two outermost poloidal field coils produces two 8 cm wide magnetic footprints, one in the upper outer divertor plate and one in the lower outer one. Additionally, a 5 mm shift of the toroidal field coils produces magnetic footprints 12 cm wide. The area of the magnetic footprints is found to be linearly proportional to the magnitude of the misalignment considered and the size of the area due to the combination of two or more error fields can be larger or smaller depending on their relative phase.

The paper is organized as follow: In section 2 there is a description of the modeling setup, in particular the M3D-C1 simulations, the TRIP3D computations and the importance of including the plasma contribution to estimate the magnetic footprints. Results are presented in section 3 for a misalignment: of the outermost poloidal field coil; of the innermost poloidal field coil; of the toroidal field bundle; and of their combination. In sections 4 and 5 a discussion of the results and the conclusions are presented respectively, and some possible future work is also introduced.

2. Modeling setup

In this section the methodology used in the study of the field line distributions on the divertor plates is presented. The first part presents the calculation of the perturbed equilibria due to misalignment of the shaping and toroidal field coils using the linear single-fluid version of the MHD code M3D-C1. The second part describes the use of the field line integration code TRIP3D to estimate the effect on the plasma footprints of such misalignment, starting from the M3D-C1 reconstructed equilibrium and using its high-resolution mesh to evaluate the local magnetic fields. The last part shows the impact of including the plasma contribution on the field line tracing results.

2.1. Perturbed equilibria from M3D-C1

NSTX-U has 14 poloidal field (PF) coils to shape the plasma column and a bundle of 12 coils to produce the toroidal magnetic field (TF). They are shown in the cutaway representation of NSTX-U in figure 1.

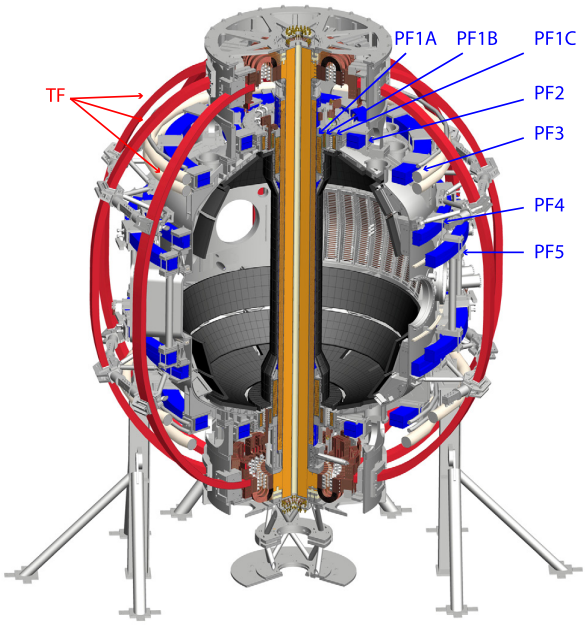

Figure 1. Cutaway representation of NSTX-U. PF1A, PF1B and PF1C indicates the 3 upper coils that are being replaced during the recovery phase (the correspondent lower coils are being replaced as well), in blue there are the other 8 shaping coils (PF) and in red the 12 coils producing the toroidal magnetic field (TF). The coils are up-down symmetric.

The effect of small shifts and tilts in the installation of the toroidal field coils bundle and shaping coils on the equilibrium field is simulated using M3D-C1. The simulations are linear since only $n = 1$ perturbations are considered (thus neglecting any shaping issue with the coils themselves and considering only error field from installation misalignments); and they are single-fluid computations. All the results presented in this paper are done for a single equilibrium case since the plasma response is sensitive to the discharge conditions and will cause changes in the results that are complicated to separate from the changes due to different coils misalignments. On the other hand, a sensitivity study to the equilibrium would be important, but it is beyond the scope of this work.

Given the up-down symmetry of the PF coils, only the misalignment of the lower coils has been considered. In particular, the results from the outermost and innermost coil (PF5L and PF1AL, where the suffix 'L' stays for 'lower') will be presented. The toroidal field coils bundle is represented as an infinitely long conductor up the center of the tokamak, and is therefore misaligned as a solid object neglecting the position of the outer legs.

2.2. Field lines tracing using TRIP3D

To study the effect that the equilibrium coil misalignments have on the magnetic field lines and their strike point, the field line integration code TRIP3D is used. Important features of TRIP3D are:

- the possibility to set the integration step size in the toroidal direction to be variable, which is very important given the low aspect ratio ($R/a \cong 1.7$) of NSTX-U, so that on the low field side (LFS), where the pitch of the magnetic field is larger, an adaptive integration step size of 0.1 degrees is used, 10 time smaller than in the high field side (HFS);
- the perturbation field is evaluated at each integration step, providing high accuracy;
- the code is specifically designed to model elongated flux surfaces in poloidally diverted plasmas.

TRIP-3D extracts the axisymmetric field from the standard EFIT [23] equilibrium file and couples it with the perturbed fields from M3D-C1 simulations, both vacuum component and plasma response. Given the linearity of these M3D-C1 calculations, the magnitude of the perturbation is scaled to desired values in TRIP3D instead of running a separate MHD simulation, thus facilitating a broad range of studies based on a small set of M3D-C1 simulations. In the recovery of NSTX-U the total misalignment (tm) of the TF and PF5 coils combined is not expected to exceed a value of tm = 6, with tm calculated as the sum of the shifts of the two coils in mm and the tilts in mrad [24]. This sets the magnitude of misalignments considered in this study, although also larger misalignments than the expected following the recovery will be shown to better illustrate the mechanism that link them to the magnetic footprints.

A similar approach used to scale shifts and tilts is used also to scale the current in the coils. Although a change in the current would also change the equilibrium, for maximum currents comparable to the simulated current the difference is negligible. In the cases presented here the equilibrium coil currents are $I_{\rm coil}^{\rm TF} = 4700$ kA, $I_{\rm coil}^{\rm PF5L} = 534$ kA and $I_{\rm coil}^{\rm PF1AL} = 387$ kA. For the TF coils this is the maximum current, for the PF5 coil this is 93% of the maximum current while for the PF1AL this is 53% of the maximum current [24]. Although for the PF1AL coil the difference in current is not negligible, it is still acceptable for the present study, since the footprints produced by its misalignment are found to be negligible compared to the other cases.

The footprints on the divertor plates are estimated both following field lines from the plasma toward the divertor plates and from the divertor plates toward the plasma, depending on the quantities to be studied. In the following sections we describe how the footprint locations are estimated when looking at the trajectory of the field lines composing them and how the footprints are estimated to compute their area.

2.3. Field loss fraction

In order to estimate the location and the size of the divertor footprints, a series of TRIP3D runs have been performed launching field lines from the plasma both toward positive and negative toroidal field directions. The former resulted in field lines hitting the upper outer and lower inner divertor plates, whilst the latter ones hit the lower outer and upper inner plates.

To choose the radial range between the separatrix and the center used to launch field lines, the perturbed equilibria

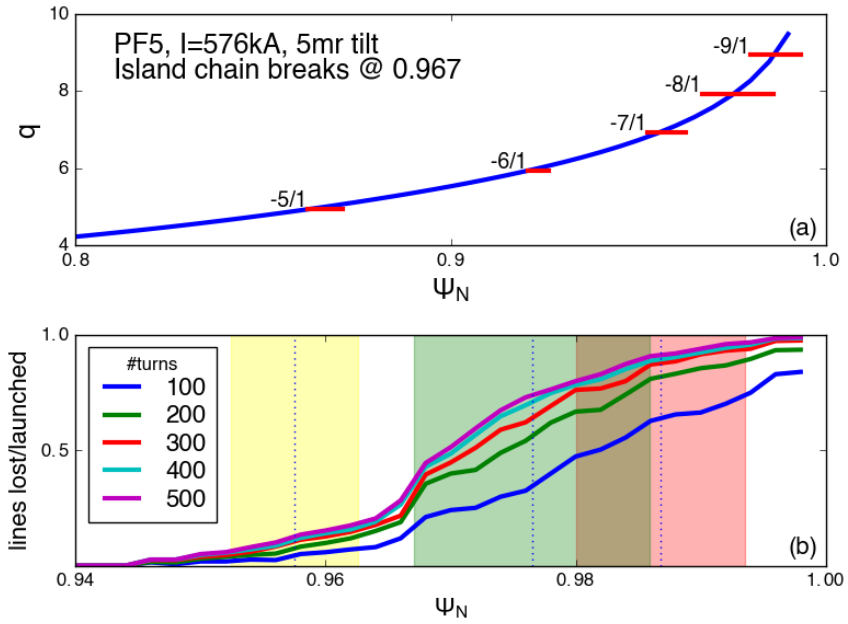

Figure 2. In (a) the radial profile of the safety factor q for the equilibrium considered. In red the island widths for a 5 mrad tilt of the lower PF5 coil as calculated by SURFMN. In (b) the ratio magnetic lines lost/launched as function of their initial normalized flux (ψ_N) starting points. The different line colors in (b) represent different TRIP3D runs with a different number of maximum toroidal turns. The vertical colored bands correspond to the width of the $-7/1$ (yellow), $-8/1$(green) and $-9/1$ (red) islands, the dotted vertical lines their center.

produced by M3D-C1 (vacuum plus plasma components) have been analyzed using the SURFMN code [25]. In SURFMN, non-axisymmetric magnetic fields are Fourier analyzed on given axisymmetric magnetic surfaces and island widths are calculated. In figure 2(a) there is an example for a 5 mrad tilt of the lower PF5 coil. Shown in blue is the q profile and in red the islands. In this example two island are overlapping, $-9/1$ and $-8/1$, and the first radial gap in the island chain is located at $\psi_N = 0.967$. This suggests that the majority of the field lines that go to the divertor plates come from $0.967 < \psi_N < 1$ in this case. In the TRIP3D simulations the first island after the islands chain is also included, to consider all the field lines going to the divertors. In figure 2(b) there are several examples of calculations done with field lines staring in the region $0.94 < \psi_N < 1$. Here the x-axis represents the initial ψ_N starting points of the field lines and the y-axis the fraction of lines hitting the divertor over the total number of lines launched from each location and the 3 color bands represent the widths of the $-7/1$, $-8/1$ and $-9/1$ magnetic islands. It is possible to see that at $\psi_N = 0.94$ no lines are lost. The fraction of lines starting at the minimum ψ_N of the $-7/1$ island ($\psi_N = 0.952$) and lost is 5.8%. It is noted that field lines lost from the $-7/1$ island across the gap with the $-8/1$ island is due to field line tunneling through heteroclinic intersection of stable and unstable invariant manifolds comprising the separatrices of these two islands as described in [15] and [16]. If $\psi_N = 0.952$ were to be chosen as minimum ψ_N, the 99.3% of the lost lines would be accounted for.

The chosen region is divided into 30 radial, 50 poloidal and 10 toroidal locations for a total of 15 000 lines launched. As mentioned previously, the integration step for each line is of 1 degree on the HFS and 0.1 degrees on the LFS. TRIP3D follows a field line until either the line crosses a previously defined boundary (the divertor in our case) or it achieves a predetermined maximum number of toroidal turns. The choice of the number of turns is fundamental for the accuracy of the calculation. In figure 2(b) the different colors of the curves correspond to the same simulation done with a different maximum number of allowed toroidal turns. In blue the simulation where lines are followed for 100 turns, in magenta a case where the lines are followed for 500 turns. It is possible to notice that the field lines have to be followed for at least 200 turns to have a converging solution and at least 400 turns to avoid the presence of fictitious structures.

2.4. Magnetic length and minimum ψ_N

An important piece of information needed to evaluate the impact that a field line has on the footprint is how long a field line stays in the plasma and how deep it goes. These are determined by the magnetic length of a field line from one divertor plate to another and by the minimum ψ_N the field line experiences. To evaluate them, TRIP3D runs are computed using the last points inside the limiter obtained by the simulations presented in the previous section as new starting point. The simulations are run for 20 000 turns to ensure all the lines are terminated by crossing a boundary surface rather than by achieving the maximum number of toroidal turns allowed.

When the tracing of a field line is interrupted by the crossing of a boundary surface, the locations of the last step inside the surface and the first step outside are recorded. The footprint is estimated from the intersection between the line connecting the two points and the divertor surface. An example of footprint in the lower outer divertor plate for a 5

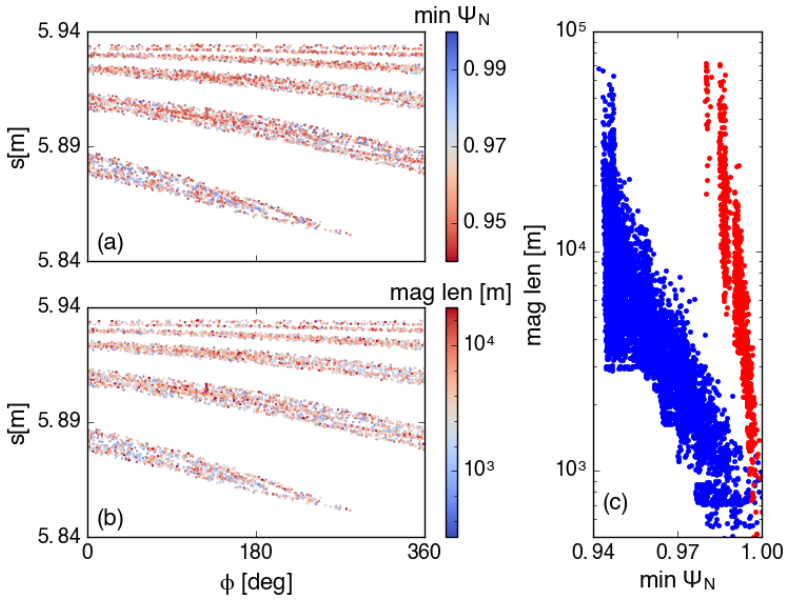

Figure 3. Comparison between the minimum ψ_N reached by a field line before hitting a divertor and its magnetic length. Panels (*a*) and (*b*) have the footprint on the lower outer divertor plate for a 5 mrad tilt of the lower PF5 coil. The hit parameter s is the distance along the wall from the HFS midplane in the clockwise direction. TRIP3D runs are done on the fields computed with M3D-C1 including the plasma response. Panel (*c*) is a comparison of minimum ψ_N and magnetic length of each dot in the footprints. The *y* axis is in a logarithmic scale. In blue for the case shown in panel (*a*) and (*b*), in red for a 1 mrad tilt of the same PF5 coil.

mrad tilt of the lower PF5 coil is shown in figure 3(*a*). Here the *x*-axis is the toroidal angle, the *y*-axis the hit parameter (*s*) and each dot correspond to the location where a field line intersects the divertor surface. The hit parameter (*s*) is defined as the distance from the inboard midplane along the limiter in the clockwise direction, as illustrated in figure 4.

The magnetic length of a field line and minimum ψ_N experienced are both used as a proxy to provide information about the energy a field line deposits to the target, so a deterministic relationship between the two is expected. Figure 3 shows a comparison between the two quantities. Figure 3(*a*) shows a footprint on the lower outer divertor plate for a 5 mrad tilt of a PF5 coil with the colors representing the minimum ψ_N experienced by each field line. Figure 3(*b*) is the same footprint, but the colors are the magnetic length on a logarithmic scale. In both these figures the white area corresponds to the region where the field lines hitting the divertor are those that stay in the scrape off layer (SOL) and never cross the last close flux surface (LCFS). Note that the footprints 'lobe' are periodic toroidally so a lobe that reaches the right boundary at 360° connects to itself on the left boundary at 0°. This shows that the footprint is generated by an $n = 1$ magnetic perturbation and has only one tip (the explicit signature of its $n = 1$ structure). Since the parallel electron thermal diffusivity $(\chi_{e\|})$ is typically 10^6 time larger that the perpendicular electron thermal diffusivity $(\chi_{e\perp})$ we do not consider SOL field lines to be significant contributors to the divertor heat flux in this analysis. Figure 3(*c*) is a comparison of the magnetic length versus the minimum ψ_N, with the magnetic length plotted on a logarithmic scale. The data in blue is from the same case shown in the other two panels, the red is for a 1 mrad tilt of the same PF5 coil. Comparing the two footprints it is possible

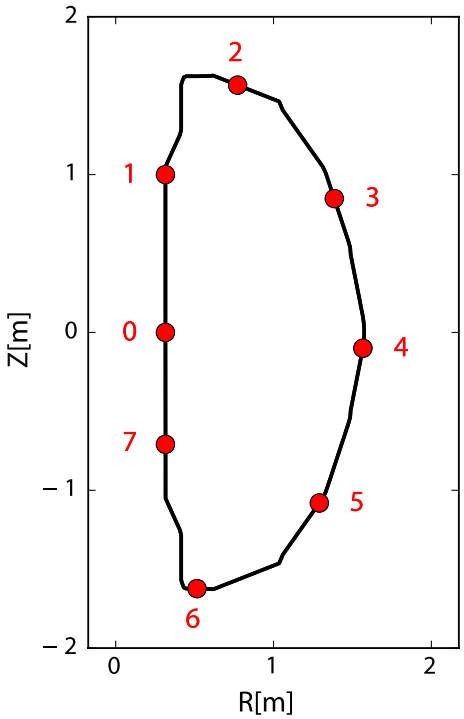

Figure 4. Poloidal cross section of the wall of NSTX-U with indicated in red a sample of the values of the hit parameter *s* in meters.

to notice that the two quantities do not have a perfect match, but they carry a similar overall information: the majority of the points are in the middle of the color scale and there are few hot spots that are diluted in the footprint. Figure 3(*c*) brings

more quantitative information. Looking at the blue points, it is clear there is an overall logarithmic dependence between the two quantities, but some features are present at the smaller ψ_N that complicate their relation. The red points highlight that in a different case there is still a logarithmic relation between the two quantities, but it is different from the first case. In particular, the range of magnetic lengths is comparable in the 2 cases, between 100 m and 100 km, while the range of minimum ψ_N is different, suggesting that the minimum ψ_N is a better parameter to compare different cases, since it also carries information about the thickness of the region of the plasma that is connected to the divertor plates.

2.5. Footprint area

Another important parameter of a footprint is its area. The punctiform nature of the field lines prevent the surface area of their footprints from being easily measurable using a conventional approach. The solution adopted here consists in creating a grid in the region of a footprint and launch a field line from the center of each grid element. The area of the footprint is estimated as a fraction of the total area of the grid equal to the ratio between number of field lines entering the plasma versus the total number of field lines launched. With such approach, there are three free parameters whose choice can impact the results: the number of turns a line is followed, the grid size, and the grid element size.

The number of toroidal turns needs to be sufficiently large to discriminate whether each line enters the plasma or not. A field line outside the separatrix cannot complete a full poloidal turn (i.e. cross the X-point), while a field line inside the plasma will. Using this definition to distinguish whether the field lines are inside the footprints, it is found that about 40 toroidal turns are needed in the cases studied for all the lines either to cross the X-point or to hit the wall.

The grid size is chosen to completely enclose the entire footprint boundaries and have at least 2 rows of lines that do not enter the plasma on each side of the grid. To choose the size of each element in the grid a series of convergence studies are done. The accepted uncertainty in the area estimation of the footprints is of $10\,\mathrm{cm}^2$. In the determination of the toroidal length of the grid all the elements are estimated to have a major radius equivalent to the mid-radius of the grid, neglecting the different radial locations.

An example of such grid for the same case of figure 3 is shown in figure 5. In blue are shown the elements of the grids from which a field line starts and stay in the SOL, in red are the field lines that enter the plasma. The vertical axis in this case is the poloidal angle of the grid elements, that goes in the opposite direction of the hit parameter.

2.6. Plasma contribution

The contribution of the plasma response to the error fields which defines the footprints has been estimated and found to be very important. This is expected since the field lines cross the unperturbed separatrix, where the fields due to the plasma response are expected to be significant [26–29]. The main effects of including the plasma response on the footprints are a change in their size and the depth of the field lines (minimum ψ_N) that penetrate into the plasma.

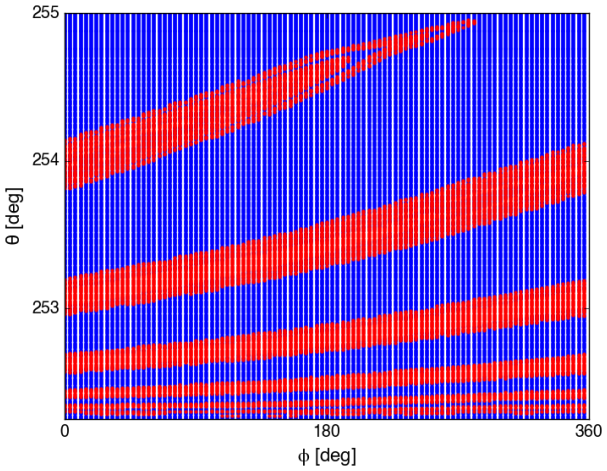

Figure 5. Grid used to estimate the area of the lower outer footprint for a 5 mrad tilt of the lower PF5 coil. Shown in red are the grid elements from which the field lines enter the plasma, while in blue are the grid elements from which the field lines stay in the SOL.

A comparison of the vacuum field and M3D-C1 plasma response footprints is shown in figure 6. Panel (*a*) and (*b*) are footprints in the outer lower divertor plate neglecting and including the 3D plasma response respectively for a 3 mm shift of the TF coils. The colors correspond to the minimum ψ_N reached by each field line. The footprint in the vacuum only case is about 12 cm wide, while it is reduced to about 6 cm in width when the plasma response is included. Moreover, the field lines go deeper in the plasma (up to $\psi_N \sim 0.85$ in the vacuum case versus $\psi_N \sim 0.95$ when the plasma response is included). Panel (*c*) and (*d*) are the footprints in the inner upper divertor plate. Here, including the plasma response produces a significantly larger footprint than in the vacuum only case. Figure 7 shows the poloidal spectrum decomposition of the field for the vacuum only case on the top and including the plasma response in the bottom, as computed by SURFMN. The two plots show that both a screening effect (for $m = nq$) and an amplification effect (for $m > nq$) are present, suggesting that the differences in size of the footprints may be due to a combination of the two effects.

Figure 8 is a comparison of the fraction of lines going to the divertor as function of their initial ψ_N with (red) and without (blue) the plasma response. This shows that, when the plasma response is included, no field lines starting inside $\psi_N \sim 0.95$ leave the plasma, whereas the vacuum only calculations predict a 50% lost fraction at $\psi_N \sim 0.95$.

In the paper all the calculations include the plasma response if not otherwise specified.

3. Results

In this section, the results of the TRIP3D simulations of M3D-C1 cases are shown. These are organized by various

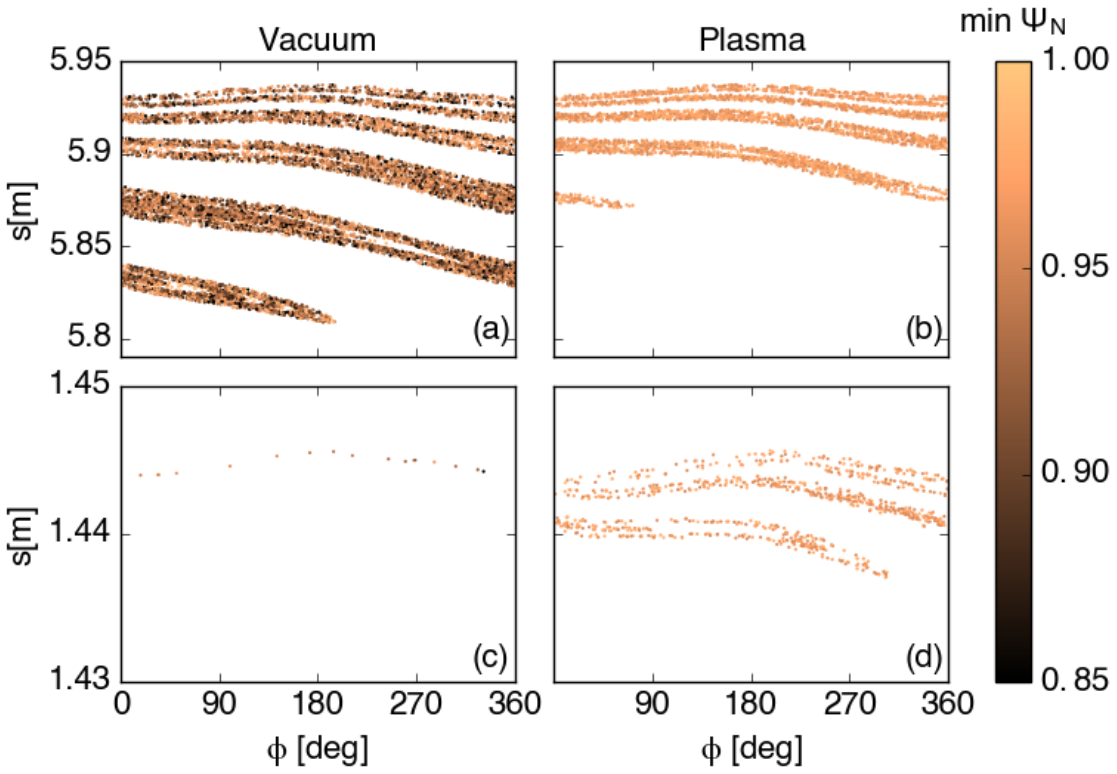

Figure 6. Comparison between the footprint in the lower outer divertor neglecting (*a*) or including (*b*) the 3D plasma response in the calculations. In (*c*) and (*d*) the same comparison for the upper inner divertor plate.

types of coil simulations PF5, PF1A and the toroidal field bundle. The first subsection deals with the misalignment of the lower PF5 coil, the second that of the lower PF1A coil and the third the misalignment of the toroidal field bundle.

3.1. Misalignment of the PF5 coil

The upper and lower outermost poloidal field coils are the primary vertical field coils. Given the upper-lower symmetry, only the misalignment of the lower coil (PF5L) is presented. The effect of a tilt, a shift as well as a combination of the two will be discussed.

3.2. Tilt

M3D-C1 simulations for a 1 mrad tilt of the PF5L coil with a current of $I_{\mathrm{PF5L}} = 534$ kA is used as a basis for the field line tracing calculation. The results are multiplied by a factor of 1.08 in the TRIP3D calculation to simulate the maximum current that can be sustained for 5 s by the coil, $I_{\mathrm{PF5L}}^{\mathrm{MAX}} = 576$ kA. The results are shown in figure 9. The plot in the middle, figure 9(*b*), is a poloidal cross section of NSTX-U with the PF coils included for reference. The tilted coil is highlighted in red. The black regions are a Poincaré plot of the field lines that go from the plasma to the divertor plates. The plots around figure 9(*b*) show the footprints. In the clockwise direction, from the top left panel, the upper inner footprint, the upper outer, the lower outer and the lower inner footprints. The colors are the minimum ψ_{N} experienced by the field lines.

Figure 9 shows that a 1 mrad tilt of the PF5 coils produces about a 1.8 cm wide footprint on each of the outer divertor plates and suggests that the inner footprints are negligible compared to the outer ones, being about one order of magnitude smaller. It also shows that the field lines hitting the divertor plates are confined to $\psi_{\mathrm{N}} > 0.98$. The SURFMN analysis shows that for such perturbation none of the $n = 1$ islands overlap.

To observe island overlapping the perturbation needs to be scaled up to at least 2.5 mrad. Figure 10 shows the ratio of the lost lines versus the launched lines as function of the initial ψ_{N}. The different panels correspond to different magnitudes of the tilt, from 1 mrad to 5 mrad. In each panel the location of the islands and their width is highlighted by the colored bands, showing the occurrence of overlap for a tilt of at least 2.5 mrad. The most interesting cases are those with the 4 mrad and 5 mrad tilts, where a step in the lost fraction is found to separate the initial ψ_{N} inside and outside the island chain. The other cases, where the overlap is not present or minimal, show a more linear trend in the lost fraction versus the initial ψ_{N}. Field lines are also lost from regions inside the minimum ψ_{N} of the last island due to tunneling effects [15].

Despite a different behavior of the lost fraction in the presence of island overlapping, the area of the footprint increases linearly with the PF5L tilt. This is shown in figure 11 in red. A 1 mrad tilt produces a footprint area of 0.018 m^2 and a 5 mrad tilt produces a 0.088 m^2 footprint. In the same plot, the inner field line loss boundary is also shown (in blue), as function of the tilt amplitude. The inner field line loss boundary

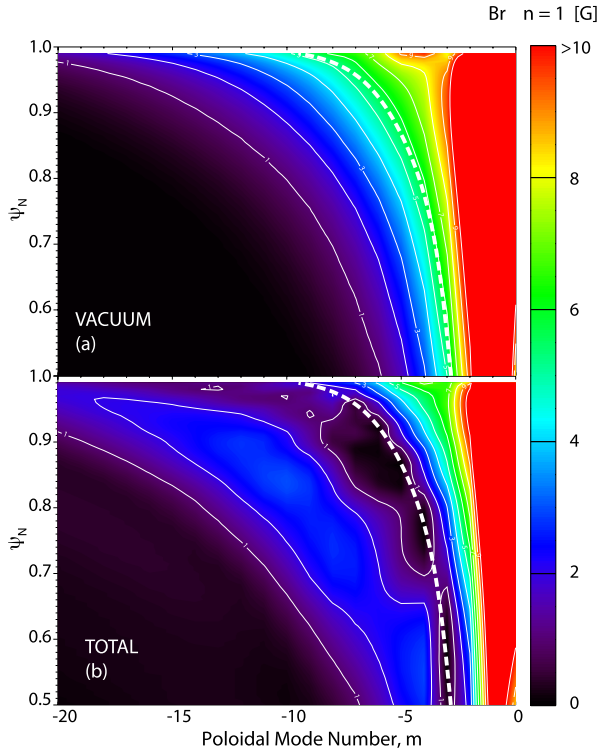

Figure 7. Contour plot of the poloidal spectrum decomposition calculated by SURFMN neglecting (*a*) and including (*b*) the contribution from the plasma response. The *x*-axis is the poloidal mode number m and the *y*-axis the normalized flux ψ_N. It is possible to see that including the plasma response results in a screening of the resonant components ($m = nq$, dashed line) and an amplification of the non-resonant components ($m > nq$, on the left of the dashed line).

corresponds to the minimum ψ_N from which at least one field line starts and reaches the divertor. As already suggested by figure 10, the larger the misalignment, the deeper the field lines can go. Moreover, for tilts greater than 2 mrad the minimum ψ_N decreases linearly and more slowly than for tilt less than 2 mrad as seen by the change in the slope of the blue curve.

3.3. Shift

Similar to what has been done for the tilt of the PF5L coils, shifts up to 5 mm have been analyzed. Both the area of a single footprint and the inner field line loss boundary for a 5 mm shift of the PF5L coil is found to be comparable to a 2 mrad tilt of this coil. This suggest that a shift of the PF5 coils is less perturbative than a tilt.

3.4. Shift and tilt combination

The M3D-C1 simulations are done for shift and tilt separately. The M3D-C1 calculations presented here are linear, so the response to a coil that is both tilted and shifted can be obtained using a linear combination of the responses to the shift and tilt of the coil calculated independently, with the appropriate amplitude and phase factors.

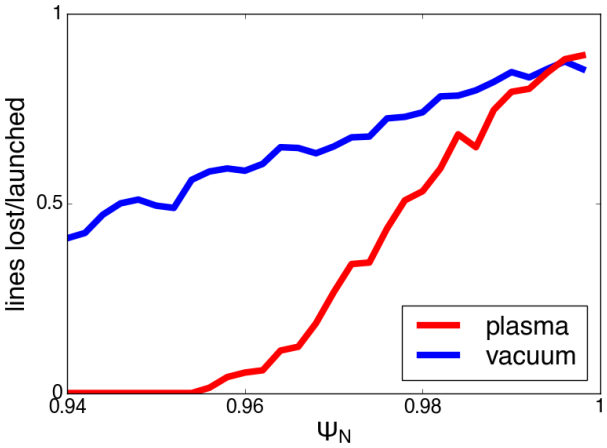

Figure 8. Ratio of the magnetic lines lost over those launched as function of their initial normalized flux (ψ_N). Shown in red is the result when the plasma response is included and in blue when neglected.

Figure 12 shows a scan of different phases between the direction of a 5 mm shift and that of a 5 mrad tilt applied to the PF5L coil. For the shift, the phase is the direction of the shift, so that a phase of 0° means a shift toward $\phi = 0°$, where ϕ is the toroidal angle. For the tilt, the phase is the direction of the axis of rotation, so that a phase of 0° means the tilt is about the axis that goes through $\phi = 0°$. For example, this would cause the PF5 coil to be higher at $\phi = 90°$ and lower at $\phi = 270°$.

Shown in red is the outer lower footprint area and in blue the corresponding inner field line loss boundary. The area goes from a minimum of 0.056 m^2 when the shift and tilt are at 30° apart to a maximum of 0.116 m^2 when the shift and tilt are at 210° apart. The largest footprint corresponds the deepest inner loss boundary, while the most superficial one is at $\phi_{tilt} - \phi_{shift} = 0°$.

3.5. Misalignment of the PF1A coil

As with the PF5L coil, a 1 mrad tilt of the PF1AL coil is predicted to have a bigger impact on the footprints than a 1 mm shift. The simulations performed however predict a negligible effect of the PF1A misalignment on the divertor footprints compared to that of the PF5L coil. The area of each of the outer footprints is about 0.001 m^2 for a 1 mrad tilt of the PF1AL coil, one order of magnitude less than the equivalent PF5L tilt.

The effect that a 5 mrad tilt of the PF1AL coil has on the footprint is shown in figure 13. In panel (*b*) there is a poloidal cross section. The striped rectangles are the PF coils, with the PF1AL coil highlighted in red. A Poincare plot of the field lines going from the plasma to the divertor plates is also shown. Figures 13(*a*) and (*c*)–(*e*) are the inner upper, outer upper, inner lower and outer lower footprint respectively. In all the cases the field lines that hit the divertor plates do not penetrate more than $\psi_N = 0.993$ and none of the footprints are more than 1 cm wide.

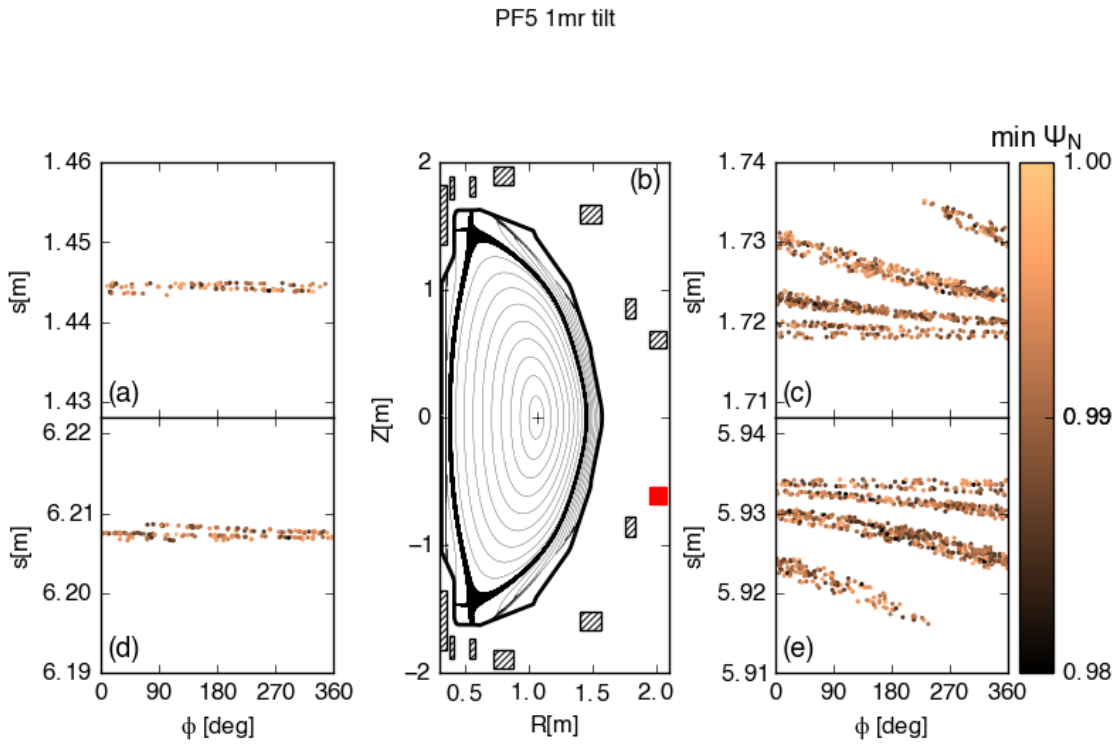

Figure 9. Figures (*a*) and (*c*)–(*e*) are the magnetic footprints due to a 1 mrad tilt of the PF5L coil in the upper inner, upper outer, lower inner and lower outer divertor plate respectively. In (*b*) a poloidal cross section of NSTX-U with the 2D equilibrium and a Poincare plot of the field lines composing the footprints. The PF coils around the machine are shown as rectangles, the red one corresponds to the misaligned one. The colors in the footprint plots (*a*) and (*c*)–(*e*) are the minimum ψ_N reached by each field line.

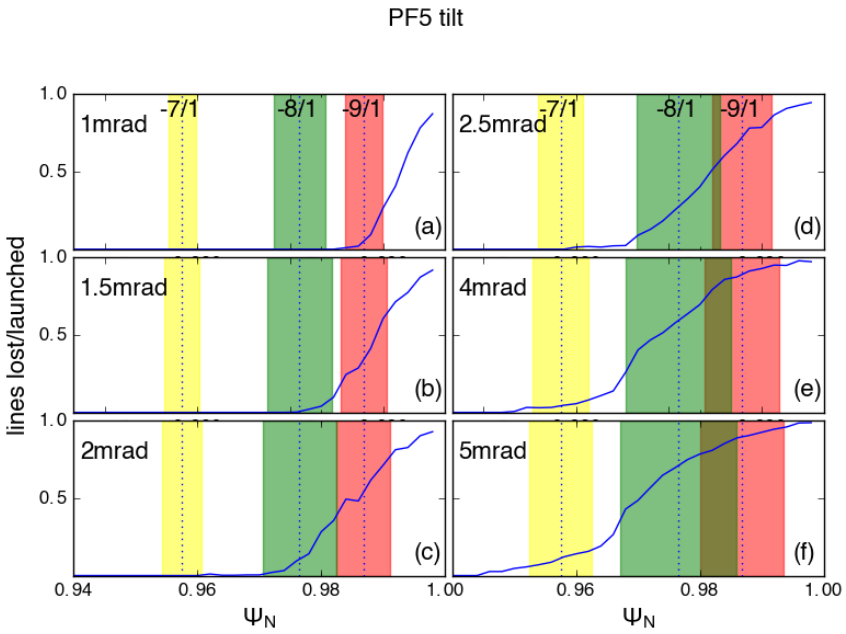

Figure 10. Ratio of the magnetic lines lost over those launched as function of their initial normalized flux (ψ_N) for different magnitudes of the tilt of the PF5L coil, from 1 mrad (*a*) to 5 mrad (*f*). The vertical shaded bands correspond to the $n = 1$ islands widths outside $\psi_N = 0.94$. The vertical dotted line corresponds to the center of the islands.

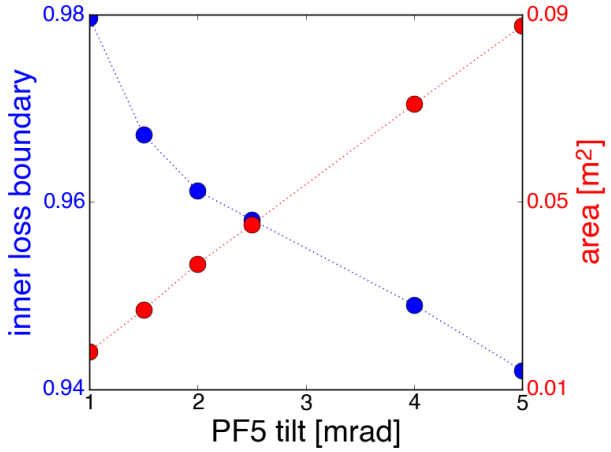

Figure 11. Shown in blue is the inner field line loss boundary as function of the magnitude of the tilt of the PF5L coil and in red the area of the magnetic footprint on the lower outer divertor.

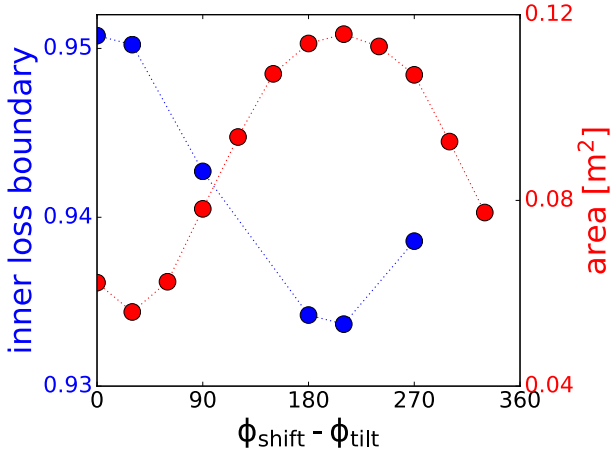

Figure 12. Shown in blue is the inner field line loss boundary as function of phase between a 5 mm shift and a 5 mrad tilt of the PF5L coil. Shown in red is the area of the magnetic footprint on the lower outer divertor.

3.6. Misalignment of the toroidal field bundle

A misalignment of the toroidal field coils is found to have a large impact on the footprints, comparable to that of the PF5L coil. In figure 14 the effect of a 1 mm shift of the TF coils with a current of 4700 kA/turn on the whole coils bundle (corresponding to $B_T = 1$ T at major radius $R = 0.94$ m) is shown. The subplots are organized in the same way as figure 13. Such a misalignment produces footprints on the outer divertor plates (figures 14(c) and (e)) between 2 cm and 3 cm wide, with field lines entering the plasma up to $\psi_N = 0.977$, while the footprints on the inner plates (figures 14(a) and (d)) are an order of magnitude smaller.

As with the poloidal field coils, increasing the magnitude of the misalignment produces an overlapping of the magnetic islands at the edge (figure 15) and a linear increase of the area of the footprints (figure 16). In figure 15 the fraction of the lines lost compared to lines launched as function of the initial ψ_N is shown. The vertical colored bands correspond to the $n = 1$ islands, in yellow the $-7/1$, in green the $-8/1$ and in red the $-9/1$. As with the PF5 case, for the smallest misalignment there is no island overlapping and the field lines that connect to the target come mainly from the $-9/1$ island, while increasing the shift magnitude causes the islands to start overlapping, generating a larger fraction of lines lost. Conversely, compared with the PF5 case, for the TF misalignment a larger fraction of lines are lost by tunneling [15] between the $-7/1$ island and the island chain given a 3 mm shift (see figures 10(e) and 15(c)). With a 6 mm shift of the TF coils, the $-7/1$ island also becomes part of the overlapping island chain and a significant tunneling is seen between the $-6/1$ and $-7/1$ islands.

In figure 16, the area of the outer lower footprint as function of the TF shift is shown in red, the inner field line loss boundary is shown in blue. While the area increases linearly with the TF shift, a more complex curve is observed for the inner field line loss boundary. A flattening of the curve from the 2 cm to the 4 cm shift and between the 5 cm and the 6 cm is observed. This is related to the number of islands forming the island chain as well as the tunneling between the innermost islands as they approach the overlap condition.

Conversely, compared to the poloidal field coils, for the TF coils the shift is found to produce a larger footprint than that resulting from a tilt. A 5 mrad tilt produces footprints with an area of 0.056 m^2, comparable to the area of a footprint produced by a 2.5 mm shift.

Combining a 5 mm shift and a 5 mrad tilt of the TF coils has an effect similar to that observed for the PF5 coil. Changes in the footprint area and inner field line loss boundary as function of the relative phase between the two misalignment is shown in figure 17. Similarly, as was shown in the PF5 case, the largest footprint with the deepest inner field line loss boundary is obtained for $\phi_{shift} - \phi_{tilt} = 180°$, while having the two perturbations in phase reduces the effect of the single misalignments.

3.7. Combining different coils misalignment

In the same way as discuss above for the combined shift and tilt of the same coil, the misalignment of different coils can be combined as well. The largest impact on the footprints is predicted to be due to a shift of the TF coils and a tilt of a PF5 coil. In figure 18 the footprint area produced by a combined 1 mm shift of the TF bundle and 1 mrad tilt of the PF5L coil as a function of the angle between their directions is shown in blue. When the PF5L tilt is at about $\Delta\phi \cong 150°$ from the TF shift, there is a sharp minimum in the resulting footprint area of ~0.004 m^2, while for a phase difference of about $\Delta\phi \cong 330°$ to 0° there is a broad maximum in the area of about 0.038 m^2. Moreover, the smallest area corresponds to the difference between the area of the two misalignments separately and the largest to their sum. This suggests a linear combination of the footprints produced by the misalignment of several coils, with the largest footprint occurring when all of them sum with each other and the smallest footprint when they cancel each other. An example of this is shown by the

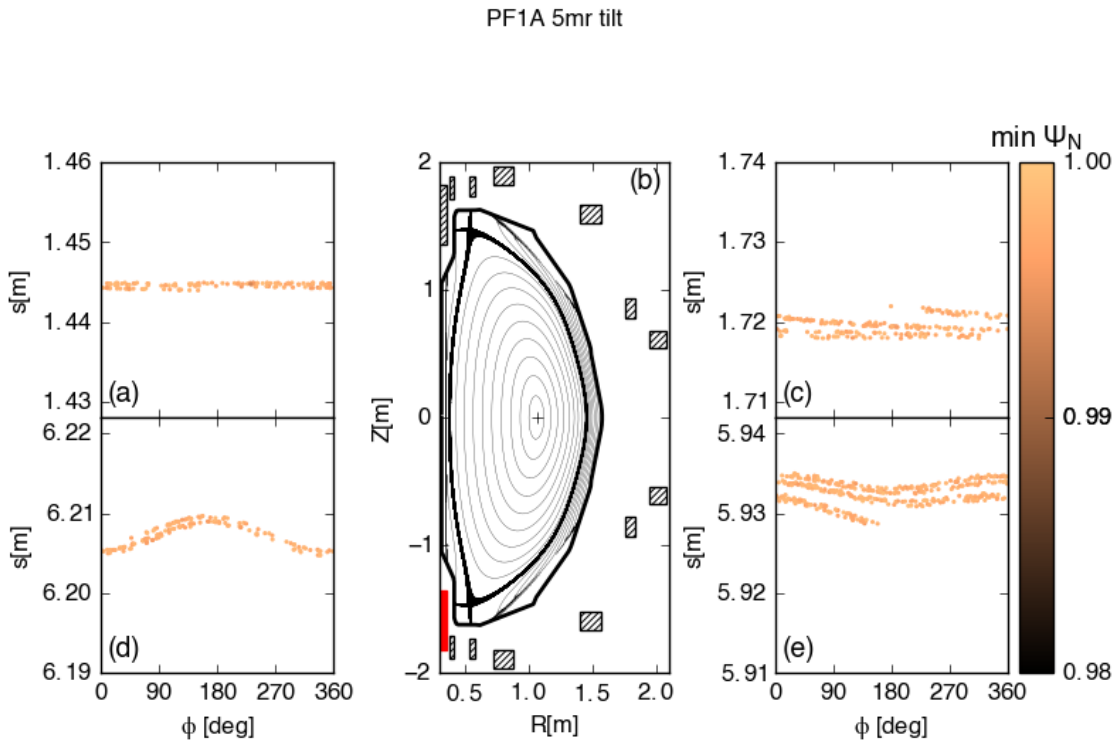

Figure 13. Figures (*a*) and (*c*)–(*e*) are the magnetic footprints due to a 5 mrad tilt of the PF1AL coil in the upper inner, upper outer, lower inner and lower outer divertor plate respectively. In (*b*) a poloidal cross section of NSTX-U with in black the 2D equilibrium and a Poincare plot of the field lines composing the footprints. The PF coils around the machine are shown as rectangles, the red one corresponds to the misaligned one. The colors indicate the minimum ψ_N reached by each field line.

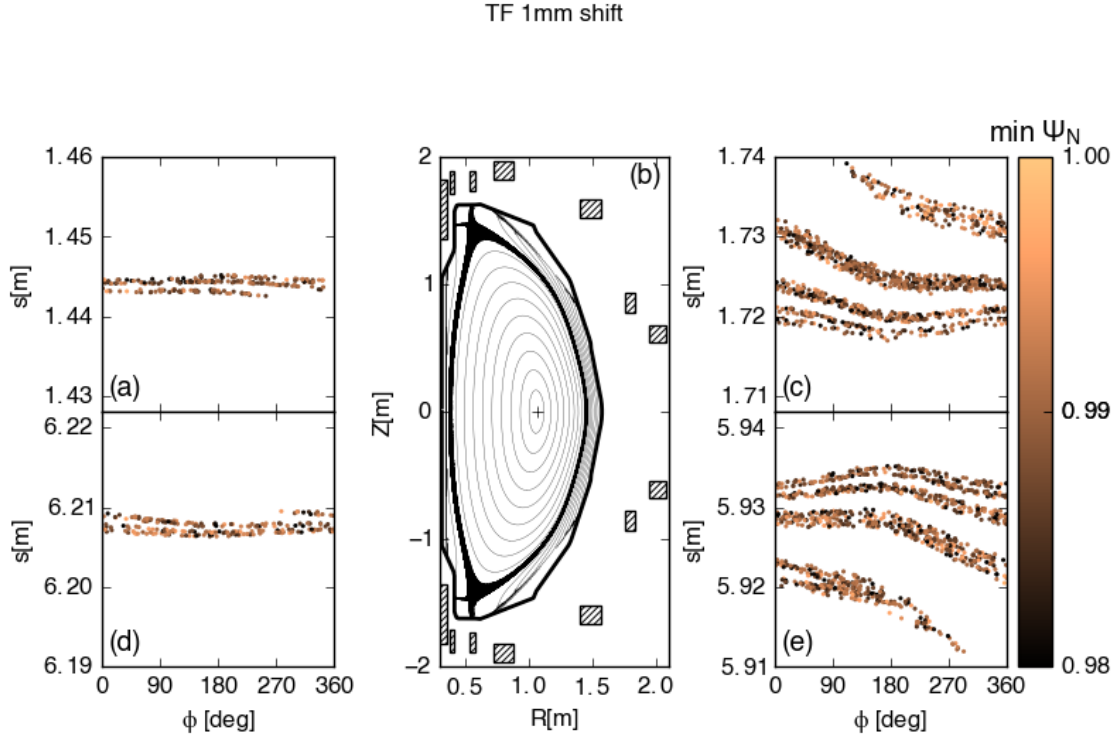

Figure 14. Figures (*a*) and (*c*)–(*e*) are the magnetic footprints due to a 1 mm shift of the TF coils on the upper inner, upper outer, lower inner and lower outer divertor plate respectively. In (*b*) a poloidal cross section of NSTX-U with (in black) the 2D equilibrium and a Poincare plot of the field lines composing the footprints. The colors indicate the minimum ψ_N reached by each field line.

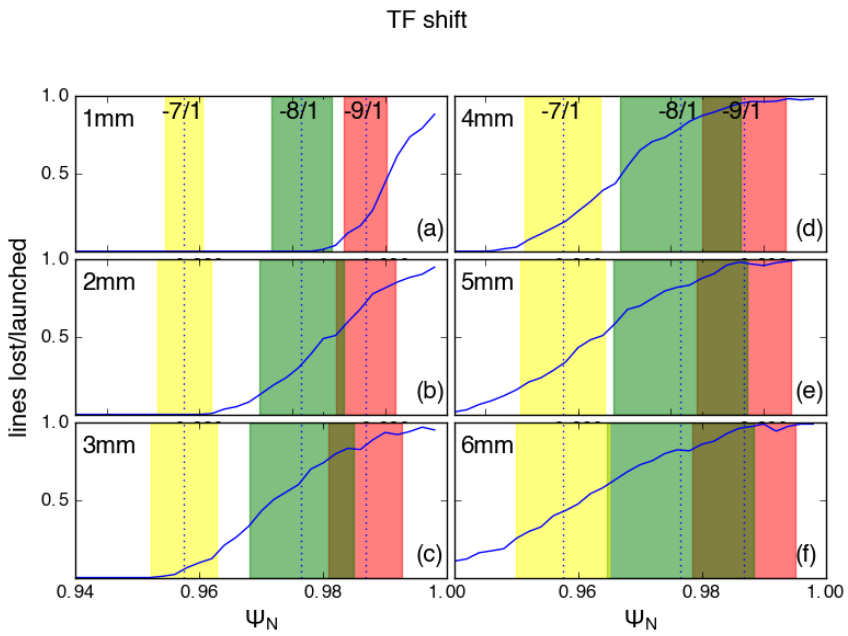

Figure 15. The ratio of the magnetic lines lost over those launched as function of their initial normalized flux (ψ_N) for different magnitudes of the shift of the TF coils, from 1 mm (*a*) to 6 mm (*f*). The vertical shaded bands correspond to the $n = 1$ islands outside $\psi_N = 0.94$. The vertical dotted line corresponds to the center of the islands.

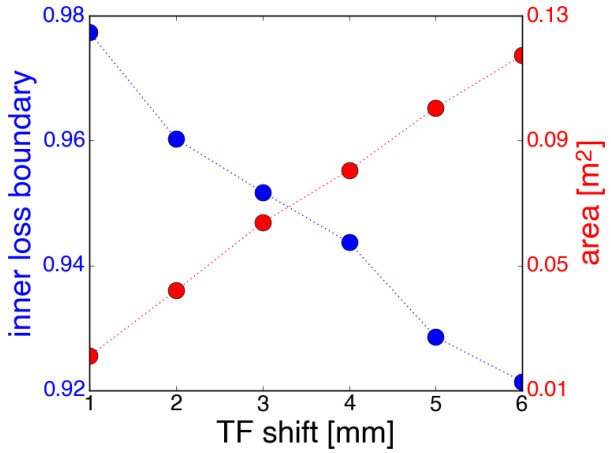

Figure 16. Shown in blue is the inner field line loss boundary as function of the magnitude of the shift of the TF coils and in red the area of the magnetic footprint on the upper outer divertor.

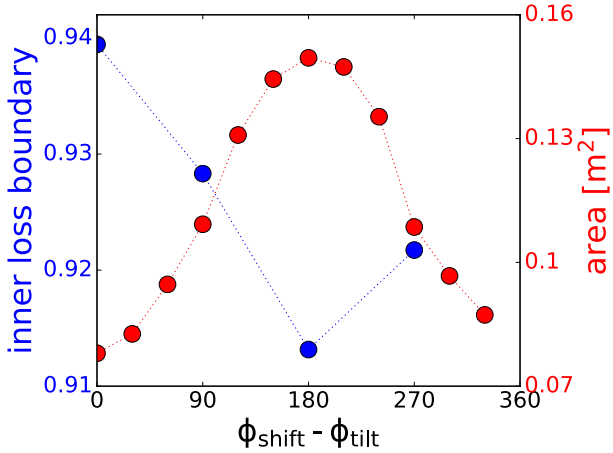

Figure 17. Shown in blue the is inner field line loss boundary as function of phase between a 5 mm shift and a 5 mrad tilt of the TF coils. In red the area of the relative magnetic footprint on the upper outer divertor.

red points in figure 18. These points represent the area of the footprint due to a 1 mm shift of the TF coils, a 1 mrad tilt of the PF5L coil at 150° from the TF shift and a 5 mrad tilt of the PF1AL coil for different phases with respect to the TF shift. For a phase of 30° the total area is about 2 cm^2, less than the uncertainty in the area calculation of 10 cm^2.

A more complex picture is derived from the inner field line loss boundary for the different relative phases. This is shown in figure 19, where the colored regions correspond to the size of three $n = 1$ islands and the dots correspond to the inner field line loss boundary. As expected, the penetration depth strongly depends on the distance among islands, so that in the majority of the phases ($\Delta\phi < 80°$ or $\Delta\phi > 230$) the minimum ψ_N is similar, between about 0.96 and 0.97, due to a large gap between the $-7/1$ and $-8/1$ islands, and it varies from about 0.97 to 0.99 when the phase is between 80° and 230°, due to the increased separation of the $-8/1$ and $-9/1$ islands at about $\Delta\phi < 150°$.

4. Discussion

Figures 20 and 21 summarize the results presented in the previous sections for individual and combinations of coil shifts and tilts. Figure 20(*a*) shows the fraction of lines lost for a 5 mrad tilt of the PF1AL coil (blue), the PF5L coil (green) and

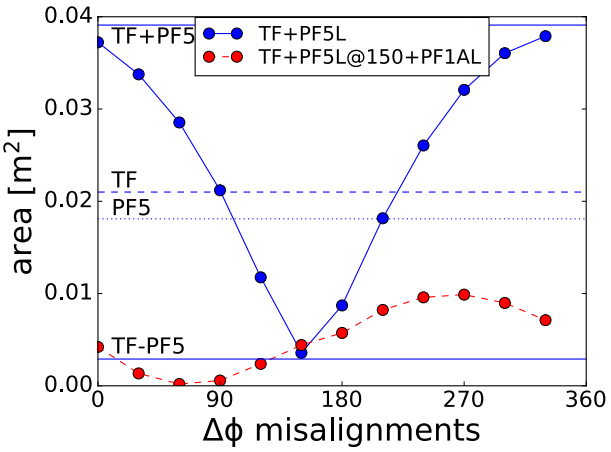

Figure 18. Shown in blue is the area of the magnetic footprint on the upper outer divertor as function of phase difference between a 1 mm shift of the TF coil and a 1 mrad tilt of the PF5L coil. Shown in red is the area of the magnetic footprint on the upper outer divertor due to a 1 mm shift of the TF coils, a 1 mrad tilt of the PF5L coil at 150° relative to the TF coil and a 5 mrad tilt of the PF1AL coil as a function of the phase between the TF shift and the PF1AL tilt. The horizontal dashed and dotted lines indicate, respectively, the area for a 1 mm shift of the TF coils and a 1 mrad tilt of the PF5L coil, the solid lines are their sum and their difference.

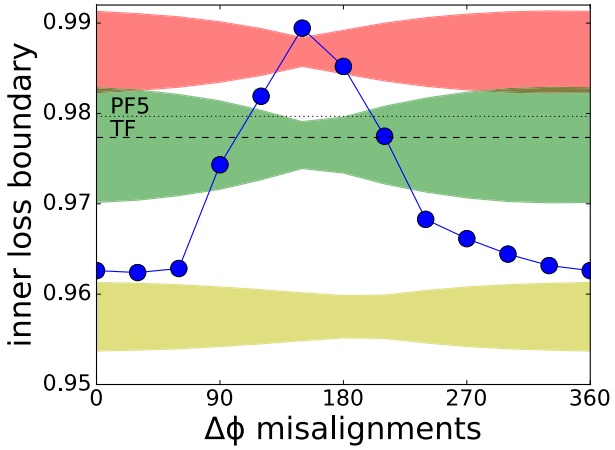

Figure 19. Shown in blue is the inner field line loss boundary for a 1 mm shift of the TF coil and a 1 mrad tilt of the PF5L coil as function of their relative phase. The shaded regions correspond to the radial extension of the magnetic islands as function of the relative phase of the TF and PF5L misalignments. In yellow the −7/1 island, in green the −8/1 and in red the −9/1. The dashed and dotted lines are the inner field line loss boundary when only one of the two misalignments is present.

the TF bundle (red), while figure 20(*b*) shows the same cases with a 5 mm shift. Three main conclusions can be drawn based on these results:

(a) a misalignment of the PF1AL coil is negligible in terms of field lines lost compared to the other two cases;
(b) a 5 mrad tilt of the TF bundle is equivalent to that of the PF5L coil, although the inner field lines loss boundary for the PF5 case is deeper;

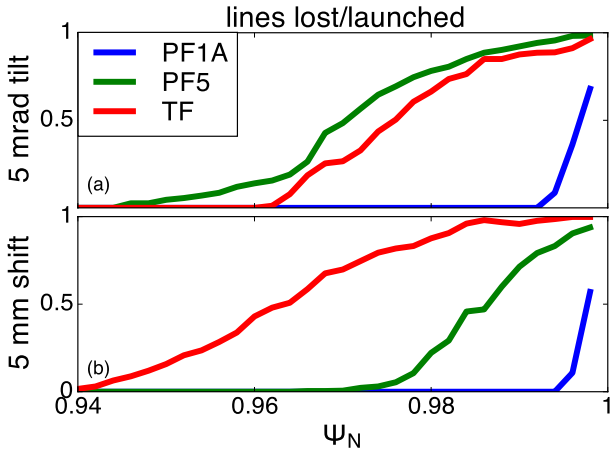

Figure 20. Ratio of the magnetic lines lost over those launched as function of their initial normalized flux (ψ_N) for a 5 mrad tilt (*a*) and a 5 mm shift (*b*) of the PF1AL coil (blue), PF5L coil (green) and TF coils (red).

(c) a 5 mm shift of the TF coils produces the largest number of lost field lines.

Figure 21 shows a comparison of the footprint areas generated by individual coils. Considering only the fraction of lines lost and the area of the footprints due to a misalignment, the effect of the PF1A coil is negligible. The areas of the footprints due to a 5 mm shift (circles) or 5 mrad tilt (triangles) of both the TF bundle and the PF5L coil are of the same order of magnitude. A shift and tilt of the same coils produces a larger footprint when they are not in phase (pentagons) compared to when they are in phase (squares).

In this work the main focus has been characterizing the magnetic footprints in terms of their size and penetration depth of the field lines composing them. A possible impact on the heat and particle fluxes on the divertor plate from these two quantities is presented hereafter, although experimental data are needed to validate this hypothesis. The size of the footprint can be considered to be inversely proportional to the heat flux, so that at a larger footprint area corresponds a larger heat flux wetted area and may result in a reduced peak heat flux compared to that of a footprint with a smaller area. This suggests that a large footprint on the divertor plates created by the misalignment of the equilibrium coils can be advantageous, although this may be more likely to produce locked modes, especially for the $n = 1$ field-errors considered here. On the other hand, a larger footprint can be detrimental because it may cause power to be deposited on regions that are not design to support high heat loads. Another possible detrimental effect is the presence of particular field lines distributions that may lead to the formation of localized hot spots inside the footprints. A qualitatively study of the penetration depth of the field lines indicates that, for the cases presented in this work, field lines that experience smaller ψ_N do not accumulate in particular spots. Although the possible presence of field lines clustering may not be a major concern for NSTX-U, since it could be mitigated by applying rotating external 3D fields, it should be further investigated in future work since

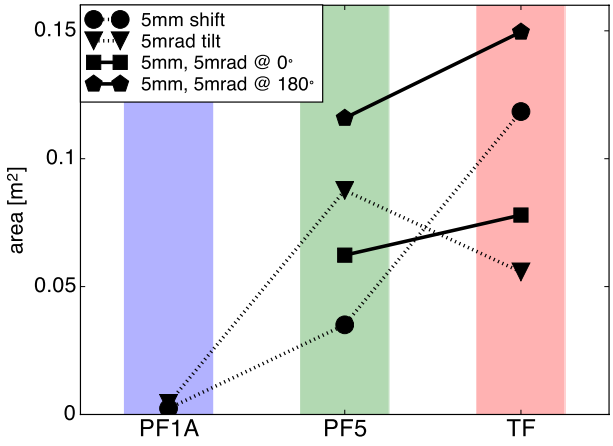

Figure 21. Summary of the magnetic footprint area for several equilibrium coil misalignments and combinations of them. On the x axis the different coils, on the y axis the area of one of the outer footprints. It is seen that, depending on their relative phase, combined misalignment that exceed the constraint tm = 6 can either produce larger (pentagons) or smaller (squares) footprints than simple misalignments within the constraint (circles and triangles).

ITER, and more in general a future fusion device, will not have such a capability. In addition, to the possibility to deposit heat flux in regions of the divertor not designed for it and to have the formation of hot spots, footprints with larger areas are made up of field lines that penetrate deeper into a hotter plasma, as shown in figures 16 and 17, which may result in a larger overall heat flux to the divertor assuming an equivalent level of radiated power along the field line path.

The estimation of how deeper field lines penetration affects the power deposited on the divertor plate per unit of area is more complex. In an ideal poloidally diverted plasma, simple two-point model that relates quantities at the divertor target plates to quantities at the midplane can be used to predict the power deposition on them. In such a model the power deposited to the target plates enters the SOL entirely via perpendicular conduction and, once in the SOL, it is quickly deposited to divertor through parallel transport. The area of the divertor target plate that is hit by the heat flux (l_t) is determined by the so-called flux expansion, so that $l_t/l_u = (B_\theta/B)_u/(B_\theta/B)_t$ where the suffix u indicates that the quantity is estimated upstream (i.e. LFS midplane) and t at the target plate. The flux expansion in the case study presented here is of about 12, so that the radial decay length of the heat flux (λ_q) at the target will be 12 times larger than that at the outboard midplane. In such conduction limited regime $\lambda_q = 2\lambda_T/7$, with λ_T the temperature radial decay length (assuming $T_e = T_i = T$). An exponential decay is usually assumed for λ_T, so that $T(r) = T_{LCFS}e^{(-r/\lambda_T)}$ [30]. The presence of small non-axisymmetric perturbations allow magnetic field lines from within the plasma to reach the divertor target plates through stochastic regions that are created between the confined plasma and the SOL, complicating the previous descritpion. In this case much of the heat coming form the plasma is trapped in the stochastic layer and reaches the divertor plates through the footprints instead of the SOL.

The radial profiles of the field line loss fraction shown in figures 10(*e*) and (*f*) are compatible with the presence of a transport barrier at the inner boundary of the island chain (ψ_N ~ 0.96). If this is the case, the energy available in the outer 4% of the plasma will be low, due to the large fraction of open field lines, and the plasma inside ψ_N ~ 0.96 will account for almost all the stored energy in the plasma. Moreover the level of radiation in the stochastic layer is also important. The radiated power is a strong function of the electron temperature (T_e). In a stochastic layer, due to the increased thermal transport, the T_e is reduced. This contributes to an increase of the radiated power and therefore to a further drop in T_e. This means that the plasma in the stochastic layer will be rather cold and highly radiative, which will reduce the convected and conducted power to the divertor [31].

It is important to stress that this is a possible basic hypothesis to interpret the field line tracing results, and a more complete interpretation of the results presented here involves a number of complex physics issues. For example, the radiation due to the stochastic layer can spread the heat flux on a larger region around the footprints [32], increasing the total amount of heat flux going to the wall and divertor. Radiative divertor operations with impurity gas injection will also reduce the heat flux inside the footprints by spreading it over a large surface area in the divertor. Experimental data are necessary to associate heat and particle flux distributions to the magnetic footprints and, therefore, guide a more detailed interpretation of these predictions. Evaluations of the total static error field in NSTX-U at the restart may be obtained through the compass scan technique [33, 34]. Data from infrared cameras and D_α cameras [35] may be then used to compare the predicted magnetic footprints with the experimental heat and particle fluxes to the divertor plates.

5. Conclusions

The main driver for the study presented here is the need to understand the impact that errors in the installation of the equilibrium coils have on the heat loads on the plasma facing components and therefore suggest the precision needed to install them. Although a large wetted area seems to be beneficial to decrease heat peaks on the wall, it must be contained in the region with the tiles designed to sustain high heat fluxes.

In this work the magnetic footprints have been used as proxy to estimate the area of the heat flux. Their size has been observed to change linearly with the magnitude of the error field and the combination of several error fields can increase or decrease it. That means that, depending on the alignment of the error field, in the worst-case scenario the resulting magnetic footprint will be the sum of all the footprints generated by the misalignment of each single coil.

In a recent trial-fit, the TF coils bundle has been installed with a precision of 0.4 mm shift and 0.14 mrad tilt [36]. If such precision can be achieved during the final installation, the error field generated by the TF coils will produce a footprint in the outer divertor plates with an area of the order of

0.01 m^2 and 1 cm wide for the particular case analyzed in this study, which is about 1/34 of the area designated for high heat fluxes in the horizontal and outer divertor regions [14,37]. Given that the largest footprints are generated by misalignment of the PF5 coil and the TF bundle, and the expectation of a maximum combined coil misalignment of $tm = 6$, the results show that the magnetic footprints will be no larger than about 10 cm if a 5.46 mrad tilt of the PF5 coil is added to the TF coil misalignment, well inside the designated area.

At this stage, however, no conclusions can be made whether the assumption that heat and particle fluxes follow the magnetic footprints is correct, as well as whether hot spots are present inside the footprints or not. Models are being developed to understand the relation between magnetic footprints and heat and particle fluxes and to predict their size at the divertor plates. Also experiments are being carried out [32] to validate them.

Acknowledgments

This material is based upon work supported by the US Department of Energy, Office of Science, under Award Numbers DE-SC0012706, DE-FC02-04ER54698[1], DE-AC02-09CH11466[2], DE-FG02-95ER54309[1] and DE-FG02-05ER54809[3]. Part of the data analysis was performed using the OMFIT integrated modelling framework [38]. The data shown in this paper can be obtained in digital format by following the links at http://arks.princeton.edu/ark:/88435/dsp011v53k0334.

Disclaimer

ORCID iDs

S. Munaretto https://orcid.org/0000-0003-1465-0971
T.E. Evans https://orcid.org/0000-0002-8357-5859
D.M. Orlov https://orcid.org/0000-0002-2230-457X
G.L. Trevisan https://orcid.org/0000-0003-4920-6109

References

[1] Buttery R.J. *et al* 1999 *Nucl. Fusion* **39** 1827
[2] Buttery R.J., De' Benedetti M., Hender T.C. and Tubbing B.J.D. 2000 *Nucl. Fusion* **40** 807
[3] Luxon J.L., Schaffer M.J., Jackson G.L., Leuer J.A., Nagy A., Scoville J.T. and Strait E.J. 2003 *Nucl. Fusion* **43** 1813
[4] Park J.-K., Boozer A.H., Menard J.E. and Schaffer M.J. 2008 *Nucl. Fusion* **48** 045006
[5] Paz-Soldan C., Buttery R.J., Garofalo A.M., Hanson J.M., La Haye R.J., Lanctot M.J., Park J.-K., Solomon W.M. and Strait E.J. 2014 *Nucl. Fusion* **54** 073013
[6] Fitzpatrick R. 1993 *Nucl. Fusion* **33** 1049
[7] Scoville J.T. and LaHaye R.J. 2003 *Nucl. Fusion* **43** 250
[8] Wingen A., Evans T.E. and Spatschek K.H. 2009 *Nucl. Fusion* **49** 055027
[9] Wingen A., Evans T.E. and Spatschek K.H. 2009 *Phys. Plasmas* **16** 42504
[10] Orlov D.M., Moyer R.A., Evans T.E., Wingen A., Buttery R.J., Ferraro N.M., Grierson B.A., Eldon D., Watkins J.G. and Nazikian R. 2014 *Nucl. Fusion* **54** 093008
[11] Trevisan G.L., Lao L.L., Evans T.E., Guo H.Y., Orlov D.M., Strait E.J., Wingen A. and Wu W. 2018 *Nucl. Fusion* **58** 026022
[12] Buttery R.J., Hender T.C., Ashall J.D., Axon K.B., Blow G. and Fielding S.J. 1996 *Nucl. Fusion* **36** 1369
[13] Menard J.E. *et al* 2012 *Nucl. Fusion* **52** 083015
[14] Gerhardt S.P. *et al* 2018 Overview of the NSTX-U recovery project physics and engineering design *Preprint: 2018 IAEA Fusion Energy Conf. (Gandhinagar, India, 22–27 October 2018)* (FIP/P3-63)
[15] Evans T.E., Chandre C., Leoncini X. and Zalavsky G. 2008 *Chaos, Complexity and Transport: Theory and Applications* (Singapore: World Scientific)
[16] Evans T.E., Roeder R.K.W., Carter J.A., Rapoport B.I., Fenstermacher M.E. and Lasnier C.J. 2005 *J. Phys.: Conf. Ser.* **7** 174
[17] Evans T.E., Roeder R.K.W., Carter J.A. and Rapoport B.I. 2004 *Contrib. Plasma Phys.* **44** 235–40
[18] Jardin S.C., Ferraro N.M., Luo X., Chen J., Breslau J., Jansen K.E. and Shephard M.S. 2008 *J. Phys.: Conf. Ser.* **125** 12044
[19] Breslau J., Ferraro N.M. and Jardin S.C. 2009 *Phys. Plasmas* **16** 092503
[20] Ferraro N.M. 2012 *Phys. Plasmas* **19** 056105
[21] Evans T.E., Moyer R.A. and Monat P. 2002 *Phys. Plasmas* **9** 4957
[22] Kalling R.C., Evans T.E., Orlov D.M., Schissel D.P., Maingi R., Menard J.E. and Sabbagh S.A. 2011 *Fusion Eng. Des.* **86** 399
[23] Lao L.L., John H.S.T., Stambaugh R.D., Kellman A.G. and Pfeiffer W. 1985 *Nucl. Fusion* **25** 1611
[24] Gerhardt S. and Park J.-K. 2018 private communications
[25] Schaffer M.J., Menard J.E., Aldan M.P., Bialek J.M., Evans T.E. and Moyer R.A. 2008 *Nucl. Fusion* **48** 024004
[26] Ferraro N.M., Evans T.E., Lao L.L., Moyer R.A., Nazikian R., Orlov D.M., Shafer M.W., Unterberg E.A., Wade M.R. and Wingen A. 2013 *Nucl. Fusion* **53** 073042
[27] Becoulet M. *et al* 2012 *Nucl. Fusion* **52** 054003
[28] Wingen A., Ferraro N.M., Shafer M.W., Unterberg E.A., Evans T.E., Hillis D.L. and Snyder P.B. 2014 *Nucl. Fusion* **54** 064007
[29] Lore J.D., Briesemeister A.R., Ferraro N.M., Frerichs H., Lyons B., McLean A., Park J.-K. and Shafer M.W. 2017 *Nucl. Fusion* **57** 056025

[30] Stangeby P.C. 2000 *The Plasma Boundary of Magnetic Fusion Devices* (Bristol: Institute of Physics Publishing)
[31] Evans T.E. *et al* 2005 *Nucl. Fusion* **45** 595
[32] Orlov D.M. *et al* 2018 Favorable impact of RMP ELM suppression on divertor heat fluxes at ITER-like conditions *Preprint: 2018 IAEA Fusion Energy Conf. (Gandhinagar, India, 22–27 October 2018)* EX/P6-17
[33] Park J.-K., Schaffer M.J., La Haye R.J., Scoville T.J. and Menard J.E. 2011 *Nucl. Fusion* **51** 23003
[34] Buttery R.J. *et al* 2012 *Phys. Plasmas* **19** 56111
[35] Moyer R.A. *et al* 2018 *Rev. Sci. Instrum.* **89** 10E106
[36] Menard J.E., Gerhardt S.P. and Feder R. 2018 Status and plans for the NSTX-U recovery project *60th Annual Meeting of the APS Division of Plasma Physics (Portland, OR, 5–9 November 2018)* (YO5.00002, http://meetings.aps.org/Meeting/DPP18/Session/YO5.2)
[37] Gerhardt S.P. *et al* 2018 NSTX-U system requirements document: plasma facing components *PPPL Tech. Rep.* NSTX-U-RQMT-SRD-003-02 PPPL, Princeton, NJ
[38] Meneghini O. and Lao L.L. 2013 *Plasma Fusion Res.* **8** 2403009